Hindawi Publishing Corporation
Journal of Nanomaterials
Volume 2013, Article ID 780125, 12 pages
http://dx.doi.org/10.1155/2013/780125

Research Article

Structure and Properties of Nanostructured (Ti-Hf-Zr-V-Nb)N Coatings

Alexander D. Pogrebnjak

Department of Nanoelectronic, Sumy State University, 2, Rymsky Korsakov Street, Sumy 40007, Ukraine

Correspondence should be addressed to Alexander D. Pogrebnjak; alexp@i.ua

Received 22 February 2013; Revised 29 April 2013; Accepted 14 May 2013

Academic Editor: Jiamin Wu

Nanostructured coatings of (Ti-Zr-Hf-V-Nb)N were obtained by the Cathodic Arc Vapor Deposition (CAVD) method. To investigate these coatings, a number of complementary methods of elemental and structural analysis were used, namely, slow positron beam (SPB), proton microbeam (μ-PIXE), micro- and nanoelectron beam (EDS and SEM analyses), and X-ray diffraction method (XRD), including method of "α-sin$^2\varphi$" measurement of a stress-strain state (X-ray strain measurement). Additionally, the texture of coatings before and after annealing up to 873 K (for time of annealing τ = 30 min) was also investigated. It was shown that increasing of stress-strain state in the coating during deposition increases the resistance to oxidation at high temperatures of annealing. It was also found that the redistribution of elements and defects, as well as their alignment (segregation), appeared due to thermally stimulated diffusion. It is also connected with the process of spinodal segregation near grain boundaries and interfaces around the grains and subgrains.

1. Introduction

Due to the low grain size (≤10 nm) and the great importance of the boundary zones (a surface boundary in particular) surrounding individual grains and nanograin joints, behavior and properties of nanocomposites crucially differ from conventional materials with the grain sizes of more than 100 nm [1–7]. Therefore, fabrication of new combinations of nanocomposite materials (nanostructured coatings) based on (Ti-Zr-Hf-V-Nb)N using cathodic vacuum-arc deposition and studies of their physical and mechanical properties turns to be a very promising trend of modern material science [7–24]. On the other hand, the theory of multicomponent high entropy alloys, which demonstrated improved thermal stability, was already proposed and demonstrated experimentally [5–7, 14, 20–23]. According to this theory, the high mixing entropy can stabilize the formation of a single-phase state in the form of a nonordered solid solution phase and prevent the formation of intermetallic phases in the process of crystallization. Thus, the fabricated highentropy alloys may feature an increased strength combined with good resistance to oxidation and corrosion. Therefore, the alloy must consist of five or more basic elements with the atomic concentration between 5 and 40%.

Thus, such elements as V and Nb, which stabilize the bcc lattice, and refractory composites of Hf, Zr, and Ti (due to their high affinity for nitrogen) [24–32] have crucial effect on formation of a nitride phase in high entropy one-component alloy.

The goal of this research is the investigation of structure and tribological properties of nanostructured (Ti-Hf-Zr-V-Nb)N coatings before and after annealing up to 873°K and also the analysis of the redistribution of defects and impurities in these coatings.

In this work, cathodes of high entropy alloys Ti-Zr-Hf-V-Nb were fabricated using vacuum arc melting in atmosphere of high purity argon. Melting was carried out by a nonexpendable tungsten electrode into a copper water-cooled tank (hearth). The obtained ingots were homogenized by 6-7 time melting with a cooling rate of 50 K/s [14].

2. Experimental Details

Deposition of coatings was performed by the cathode vacuum-arc deposition method on the apparatus Bulat-6 [1] under constant negative potential U_s = (−40–200) V, which was applied to a substrate. The arc current did not exceed 85 A, and the pressure of residual gas was 0.0066 Pa. Deposition conditions, which were employed for all of samples, are presented in Table 1.

Thermal annealing of coatings was performed in the furnace VacuTherm-Ceram VT 1200 at temperature 873 K for 30 minutes. Residual pressure P was 100 Pa.

The elemental composition was studied with scanning electron microscope (SEM) with EDX microanalysis JEOL-7000 F (Japan). To perform the element analysis over a sample depth, we employed the Rutherford backscattering (RBS) method with He^+ ions of 1.7 MeV (the scattering angle was $\theta = 170^\circ$) with a normal fall of probing ions to the surface of coated samples. The energy resolution of detector was 16 keV. A dose of helium ions was 5 μ Ci. To interpret the RBS spectra and to obtain the element profiles over the coatings depth, we employed standard software [24].

A positron annihilation spectroscopy (PAS) (Halle, Germany) was used for analysis of vacancy type defects in the coating. Using slow positron microbeam was obtained by positron annihilation energy spectra, which let us calculate an important characteristic of material, the S-parameter of Doppler broadening of an annihilation peak. It depends on energy of the incident positron beam (30 keV), that is, on the depth of the analysis [33].

Proton microbeam (μ-PIXE) was employed for elemental analysis of coatings. The initial energy of an electrostatic accelerator IAP (Sumy) was 1.4 MeV with the beam size of 0.4 μm (the charge was 3×10^{-10} C/pixel, the raster was 50 × 50, and the step size was 0.5 μm) [34]. We obtained maps of the elements Ti, Zr, Hf, V, Nb distribution before (as deposited) and after annealing up to 873 K.

The phase composition and structural studies were performed on the X-ray diffractometer DRON-3M and Rigaku RINT-2500, MDG Japan, in the filtered radiation of Cu-Ka using in the secondary beam graphite monochromator. The diffraction spectra were surveyed in the point-by-point scanning mode with a step $2\theta = 0.05$–0.1°. We also employed the diffraction of X-rays using a grazing incidence beam, in Cr emission, at angle 3°. In order to study the stress-strain state of the coatings, we employed the method of X-ray strain measurements ("α-$\sin^2\varphi$" method) and its modifications, which are commonly applied to the coatings with strong axial texture [10–14].

Tribological tests were performed on automated friction machine "Tribometer," CSM Instruments in air by "ball-disk" scheme at 293 K. The ball with diameter of 6 mm was made of sintered certificated material-Al_2O_3. The coatings were deposited on steel (45 HRC = 55) discs with a diameter of 50 mm and a thickness of 5 mm. The load was 3.0 N, sliding velocity 10 cm/s.

3. Results and Discussion

The (Ti, Hf, Zr, V, Nb)N coating had a face-centered cubic (FCC) crystal structure rather than coexisting separated nitrides. TiN, HfN, ZrN, VN, and NbN had an FCC structure. Thus, the (Ti, Hf, Zr, V, Nb)N coating also exhibited an FCC solid solution structure, in which the Ti, Hf, Zr, V, and Nb atoms were randomly distributed over the metal sublattice. The same phenomena were also reported for as-deposited mixtures of FCC forming multiprincipal element nitrides such as AlCrTsTiZr [35], AlCrNbSiTiV [36], and TiVCrZrY [37]. This result not only implied the formation of a solid solution from all constituted nitrides, but also confirmed the effect of high mixing entropy on the simplification of the crystal structure.

The solid solution phase with an FCC structure was also thermodynamically stable because it did not decompose or form other compounds even during annealing up to 873 K for 30 min. The stability of the FCC solid solution phase was also due to the high entropy effect. In addition, as shown in the paper, the crystal size and lattice constant are shown.

Based on RBS, EDX, and XRD information, the composition variation and phase separation can be excluded since the composition and structures of coating hardly had any change. The stress relaxation of as-deposited coatings after annealing has been noted from a shift in the XRD peak position. This finding is attributed to the diffusion of implanted atoms to the surface, hence the annihilation of the stress-inducing defects, as will be shown using results of measurement of Doppler broadening of the annihilated peak (DBAP) of slow positron beam. Accordingly, the lattice decline was believed to result from a release of intrinsic microstress.

The morphology of coating surfaces and the element distribution were studied using the scanning electron microscope with EDS analysis JEOL-7000 F.

Figure 1(a) shows the distribution of elements on the surface of samples in elemental contrast. Integrated analysis was obtained from the area of 0.1 mm × 10 mm. The intensity of the color indicates the concentration of elements. The dark spots on the surface of coating are the drop fraction, which appeared during the deposition of coating. Figures 1(b) and 1(c) show results of microanalysis (EDX) of coatings obtained under different deposition conditions, and Figure 1(d) shows results of microanalysis after annealing 873°K (for 30 min, at pressure in chamber 100 Pa).

As you can see from these results the element concentration in the coating is N = 49.05 at.%, Ti = 22.92 at.%, V = 5.04 at.%, Zr = 6.84 at.%, Nb = 7.47 at.%, and Hf = 8.68 at.% at pressure 2×10^{-2} Pa. When the pressure decreases to 3×10^{-2} Pa, the spectra indicate a reduction of the specific content of the nitrogen atoms in the coating composition to N = 36.04 at.%, Ti = 20.13 at.%, V = 2.28 at.%, Zr = 17.12 at.%, Nb = 17.50 at.%, and Hf = 6.93 at.%. It means a significant deficiency of nitrogen atoms in nitrides of the multicomponent systems in comparison with stoichiometric ones at high pressure 3×10^{-2} Pa. The results of RBS (Figures 2(a) and 2(b)) and EDX analyses indicate a crucial effect of the radiation factor (achieved by increasing of negative bias potential applied to the substrate) on segregation processes

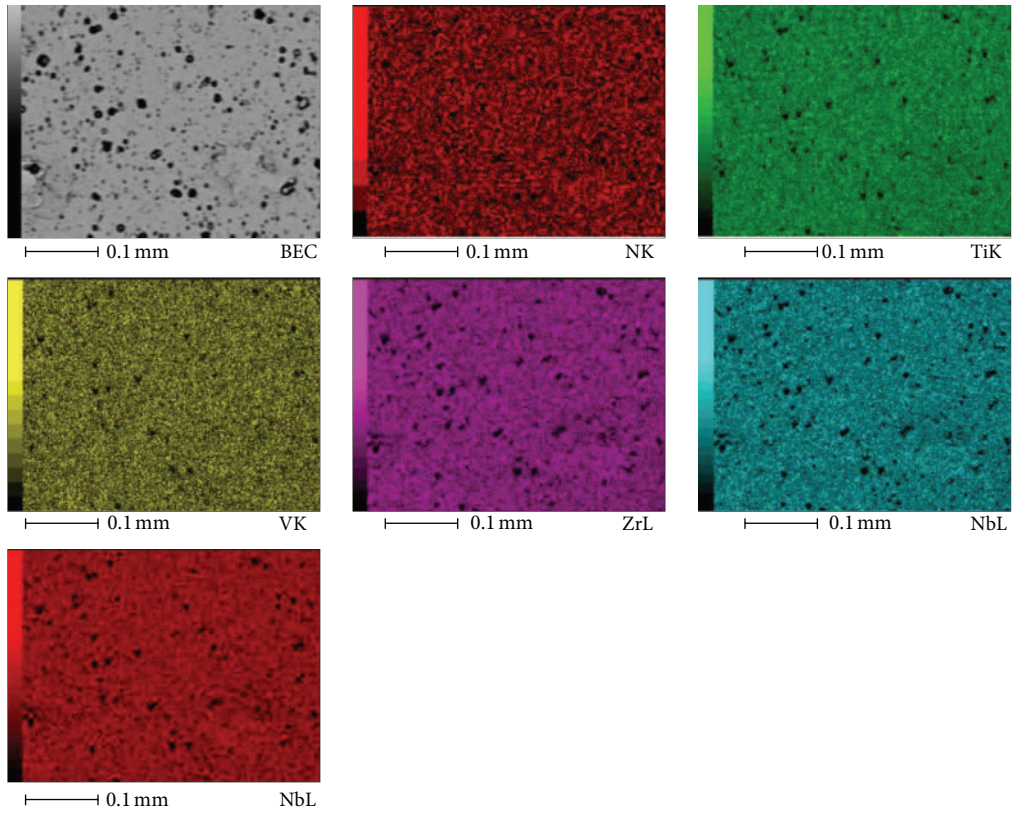

(a)

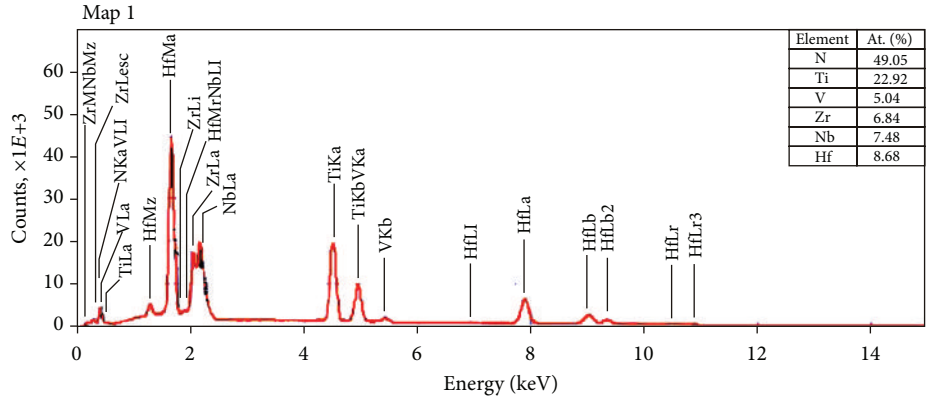

(b)

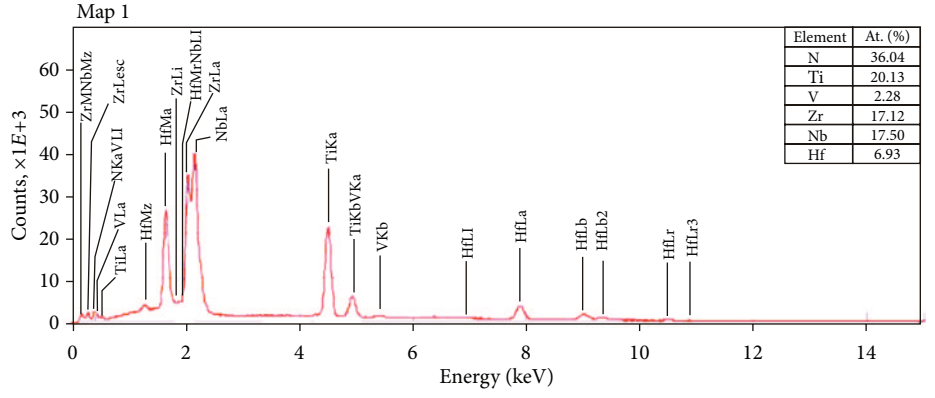

(c)

Figure 1: Continued.

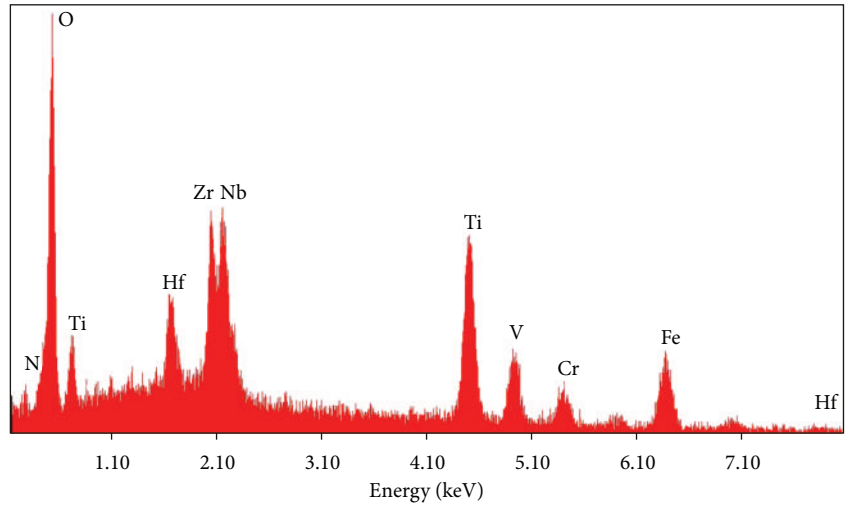

(d)

FIGURE 1: Images obtained by the scanning microscope JEOL-7000 F: (a) is the coating surface in reflected electrons; (b) shows microanalysis of coatings, N, Ti, V, Zr, Nb, obtained under $U_{bias} = -100$ V, pressure $P = 2 \times 10^{-2}$; (c) shows microanalysis of coatings, N, Ti, V, Zr, Nb, obtained under $U_{bias} = -200$ V, pressure $P = 3 \times 10^{-2}$; (d) shows microanalysis of coatings, N, Ti, V, Zr, Nb after annealing 873 K (for 30 min, at pressure in chamber 100 Pa).

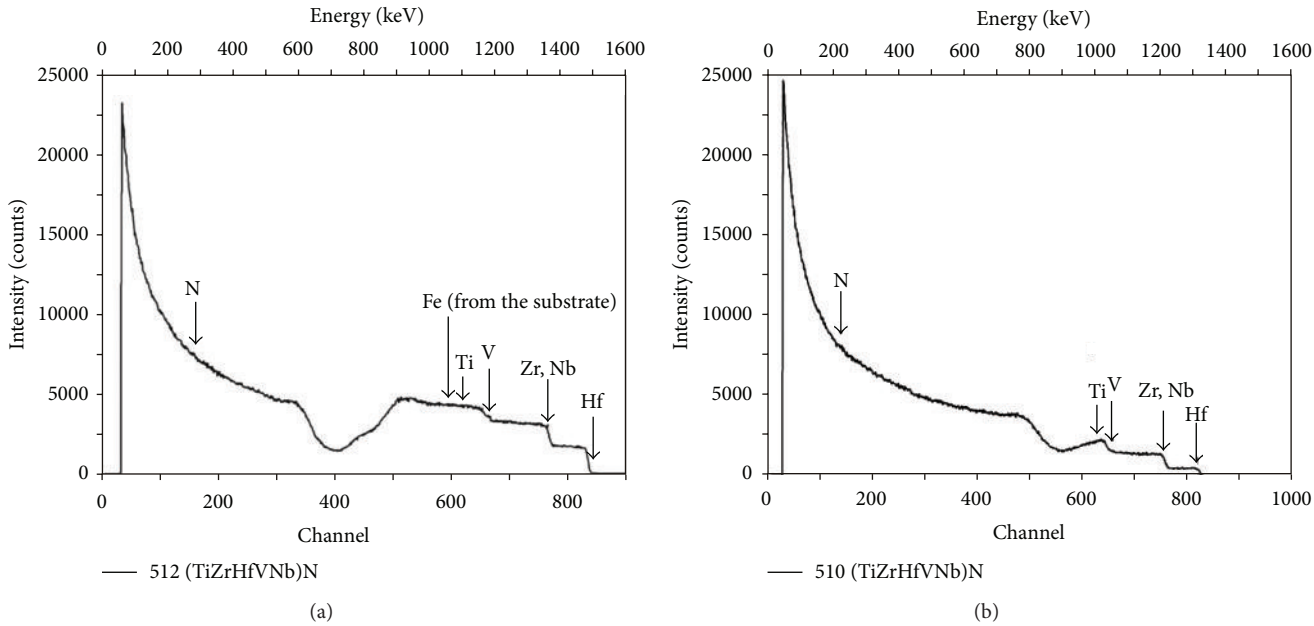

FIGURE 2: Results of the analysis of RBS spectra from samples 512 (a) and 510 (b).

arising during coating deposition. In other words, the energy of ion plasma flux increases due to the rising bias potential, which enhances the contribution of the radiation factor. It is known that the formation of a two-phase nanostructured film requires two terms: (1) the increased rate of atomic diffusion along the grain interfaces and (2) the high temperature of 873°K in the process of deposition to complete the process of spinodal segregation [18, 19, 26].

From results of EDX analysis (see Figure 1(d)) after annealing of coatings, an oxide film is forming on the surface. It is also confirmed by XRD analysis of this sample presented in Figure 5(b). The appearance of elements Fe and Cr on EDX spectra can be explained by diffusion of these elements from substrate (which is made of steel). The deviation of the values of N concentration in coatings was not more than 0.26 at.% for coating with concentration of N = 49, 05 at.% and not more than 0.18 at.% for coatings with concentration of N = 36.05 at.%.

PAS experiments demonstrated that positrons are well localized in the areas of low electron density (i.e.,

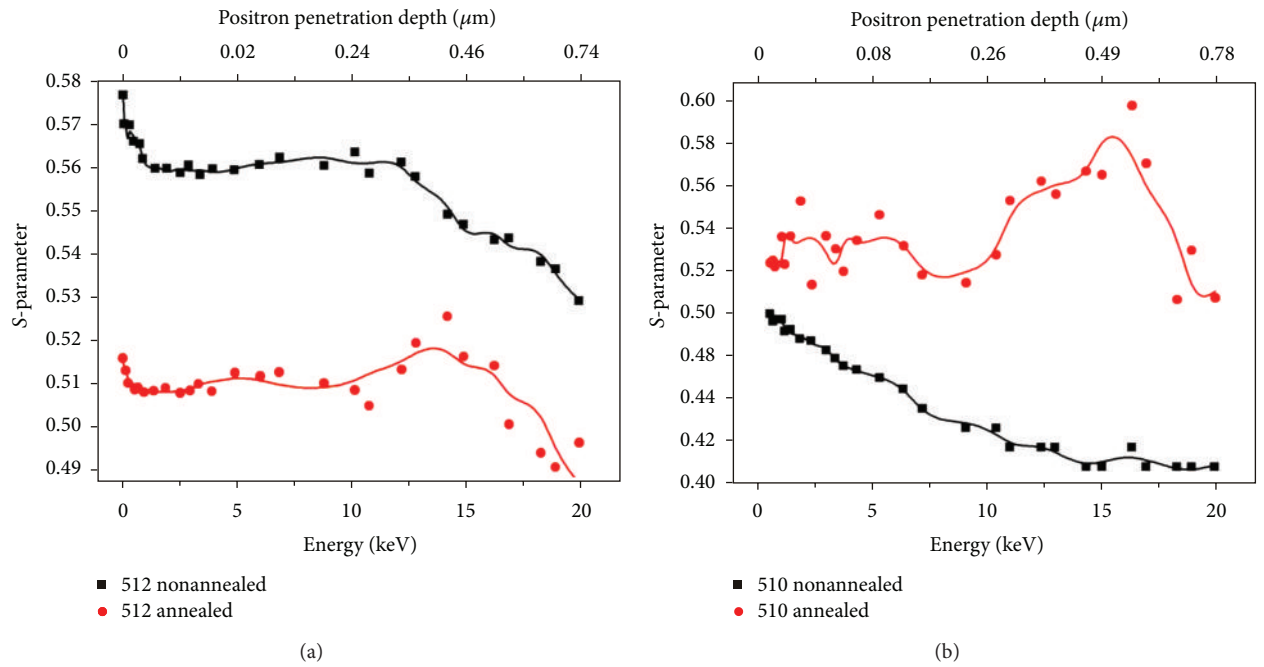

Figure 3: Dependencies of the *S*-parameter of the annihilation peak Doppler broadening measured over (Ti-Zr-Hf-V-Nb)N coating depth, for the samples 512 (a) and 510 (b), after deposition and annealing at 873 K, (100 Pa).

Table 1: Parameters of deposition and concentration of obtained coatings using C-PVD (concentration was measured using EDX-JEOL-7007F).

No.	Material	U_{bias}, V	P, Pa	Concentration, %					
				N	Ti	V	Zr	Nb	Hf
505	TiZrHfVNbN	110	0.5×10^{-1}	49.15	16.63	5.91	8.17	8.88	11.26
506	TiZrHfVNbN	100	0.2×10^{-1}	49.05	22.92	5.04	6.84	7.47	8.68
507	TiZrHfVNbN	50	5×10^{-2}	51.13	25.31	4.72	5.70	6.31	6.84
509	TiZrHfVNbN	100	3×10^{-1}	44.7	25.31	4.57	7.60	7.99	9.83
510	TiZrHfVNbN	50	2×10^{-1}	49.11	19.67	5.65	7.68	8.24	9.64
512	TiZrHfVNbN	200	8×10^{-2}	46.65	17.03	2.79	12.01	12.54	8.98
513	TiZrHfVNb	40	8×10^{-2}	—	34.66	8.88	19.53	23.16	13.76
514	TiZrHfVNbN	200	2×10^{-1}	47.69	16.41	1.93	13.34	13.90	6.72
515	TiZrHfVNbN	200	3×10^{-2}	36.05	20.13	2.28	17.12	17.50	6.93
523	TiZrHfVNbN	200	2×10^{-1}	43.44	17.80	1.45	16.39	16.99	3.92

vacancy-type defects divacancies, conglomerates of various vacancies, vacancy complexes, and plus two or three interstitial atoms [26–29]). As it follows from [27–32], the nanostructured materials, fabricated using the compaction, are good traps for positrons, which then annihilate with two or three components of the positron lifetime τ_2, τ_3. It is associated with positron annihilation at the grain interfaces, that is, the quasi-amorphous phase, in our case. The presented results (Figures 3(a) and 3(b)) clearly indicate that the defect profiles (*S*-parameter) significantly differ for various deposition conditions; see, for example, samples 510 and 512. At the same time, thermal annealing in a chamber with at high enough residual pressure (100 Pa) leads to even greater changes of the *S*-parameter over the coating depth. The value of *S*-parameter for the sample 512 decreases from 0.58-0.56 to 0.52-0.51 after annealing, and only when the analyzing energy of positrons approaches (12.5–15) keV, it increases to 0.53. Analysis of *S*-parameter curve of the nonannealed sample 510 (3b) allows to conclude that positron-sensitive defects are almost absent throughout the whole coating depth. This means that annihilation occurred mainly with the electrons of the defect-free areas. Therefore, the value of *S*-parameter was minimal and equal to 0.49. As a result of annealing at 873 K, the value of *S*-parameter increased significantly to 0.53 in the surface layer of the coating. The value of *S*-parameter further increased at positron energy of 14 to 17 keV and approached the maximum possible value 0.59.

It should be mentioned that the *S*-parameter depends on both the concentration and the type of vacancy defects,

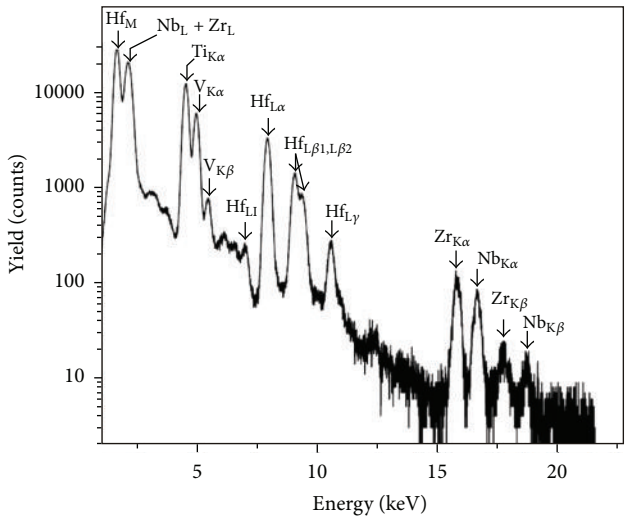

Figure 4: A common PIXE spectrum (in a logarithmic scale) obtained from a sample of the 512, when it was irradiated by a proton beam of 1.4 MeV energy.

at which positrons are captured and subsequently annihilate there in the areas of low electron density [27–29].

Since a grain size of the nanostructured coatings is smaller than a length of positron diffusion track in defect-free nanograin, all positrons can reach the grain surface and consequently the interfaces. In this case, most of the volume of available information concerns the defects in the interfaces and triple or more joints. Since the grain size in our experiments varies from 40 to 60 nm, the volume fraction of the interfaces may reach 30 to 35 vol.%, and the interfaces of triple joints may be about 5 to 10 vol.%, and then almost all positrons have to be captured along the interfaces [27].

According to results presented in [32], the total fraction of interfaces can be evaluated as

$$V_{\mathrm{Si}} = 1 - \frac{[3S \cdot (L/S)]}{L^3} \approx \frac{3S}{L}, \quad (1)$$

where L is the grain size and S is the interface width (the near-interface zone). A fraction of the inherent grain interfaces is

$$V_{\mathrm{Ii}} = \frac{[3S \cdot (L/S)]}{L^3}, \quad (2)$$

And a fraction of triple joints is

$$V_{\mathrm{Ti}} = V_{\mathrm{Si}} - V_{\mathrm{Ii}}. \quad (3)$$

If the distance between the defects is essentially shorter than the positron diffusion length, all positrons have to be captured by defects; that is, we observe the capture saturation. In this case, the positron lifetime spectrum contains only one component [27, 28], and the S-parameter of Doppler broadening seems to have a maximum value.

Figure 4 shows the integral spectrum obtained by PIXE of the element concentrations for (Ti-Zr-Hf-V-Nb)N coatings number 512 after annealing at 873 K (30 min). We can evidently see the redistribution of elements over depth after thermal annealing. Studying these spectra, we found all the elements constituting the nanostructured coating. As it will be shown later in the text, the μ-PIXE element distribution maps taken from the (Ti-Zr-Hf-V-Nb)N coating before and after annealing up to 873 K in Figures 7(a) and 7(b) can be seen.

The X-ray diffraction data for the sample 512 shows formation of a strong texture with the (111) axis, which is perpendicular to the plane of growth (Figure 5). The data of X-ray strain measurements indicate that the samples 512 are characterized by the highest value of a lattice period in a stress-free cross-section (a = 0.442 nm). It correlates with the results of elemental analysis, according to which the highest concentration of nitrogen is observed when the working pressures of coating deposition are high.

An appearance of biaxial texture with (111) and (110) axes at $U_{\mathrm{bias}} = -200$ V resulted in formation of coatings with the highest hardness reaching 58 to 60 GPa and very uniform and smooth surfaces [29–32].

In this case, thermal annealing does not significantly change a structure-phase state of the coatings (Figure 5(a)). However, it reduces a little the deformed state of compression from the strain ratio of 2.76% in initial state (as-deposited state) to 2.59% after annealing.

It was found that there was only a slight increase from 56 nm to 68 nm of crystal size and a decrease from 0.4424 Å to 0.4386 Å of lattice constant, with an increase of annealing temperature from RT to 873 K. The barely changed structure and grain size during high temperature annealing are believed to be attributed to the small driving force because of the low grain boundary energy and low kinetics from the sluggish diffusion. The grain boundary energy comes from the energy difference between the state of grain boundaries and that inside the grains. The large lattice distortion effect because of large atomic size difference (the atomic size Ti, 1.462 Å; V, 1.316 Å; Zr, 1.603 Å; Hf, 1.578 Å, Nb, 3.301 Zr, 1.603 Å; Hf, 1.578 Å) can markedly raise the overall free energy of crystalline structure.

Therefore, the actual grain boundary energy was largely lowered, leading to very small driving force for coarsening. A detailed mechanism has been proposed by Huang and Yeh [36] in case of (AlCrNbSiTiV)N coating. The sluggish diffusion originating from the higher packing density because of the packing of atoms with different sizes made the effective diffusion distances very short, which led to the enhanced difficulty of grain growth. Regarding the lattice decline, the following three possible factors must be considered: composition variation, phase separation, and residual stress.

At lower pressures of deposition P_{N} = 0.1, the decrease of the lattice period in a stress-free sections was observed at 0.438 nm, which seemed to be associated with a lower content of nitrogen atoms in the coating. Annealing of the samples 510 not only led to a significant change of the stress-strain state but also of the phase composition (see Figure 5(b), curve 2).

These figures show that samples number 510 demonstrate a decrease of the intensity of textured reflexes of an FCC metallic crystal lattice (compare spectra 1 and 2 in Figure 5(b)). In this case, nitrogen atoms are in the form of

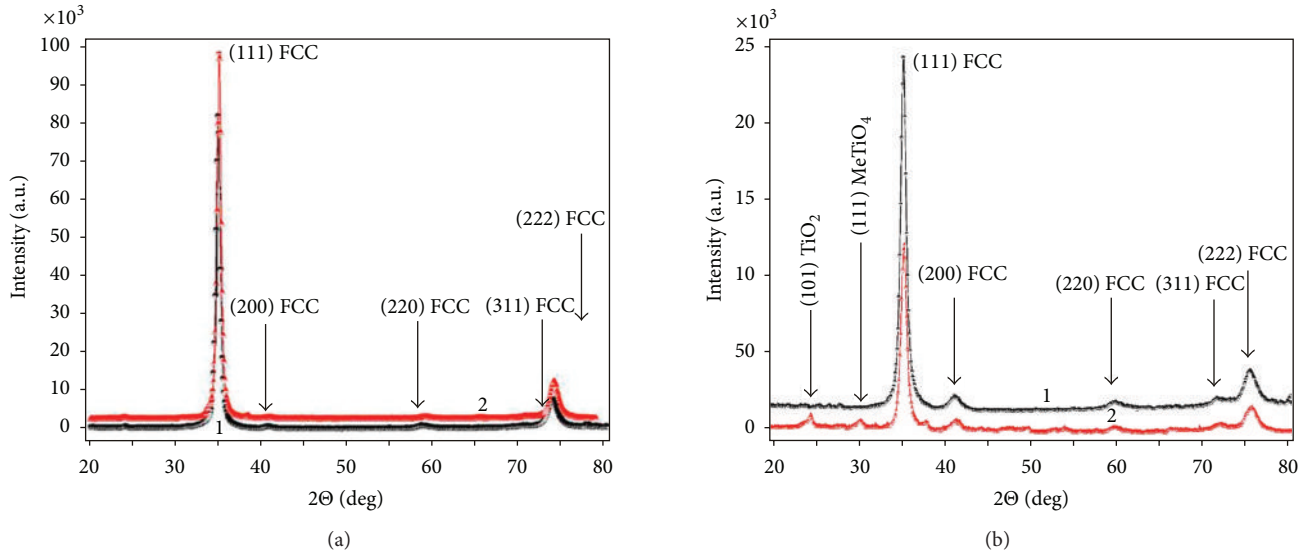

FIGURE 5: (a) The XRD spectra for a coating fabricated at $P_N = 0.7$ Pa and $U_b = -200$ V (sample 512): (1) before annealing; (2) after thermal annealing. (b) The XRD spectra of a coating fabricated at $P_N = 0.2$ Pa and $U_b = -50$ V (sample 510) before annealing (1) and after thermal annealing at 873 K (2).

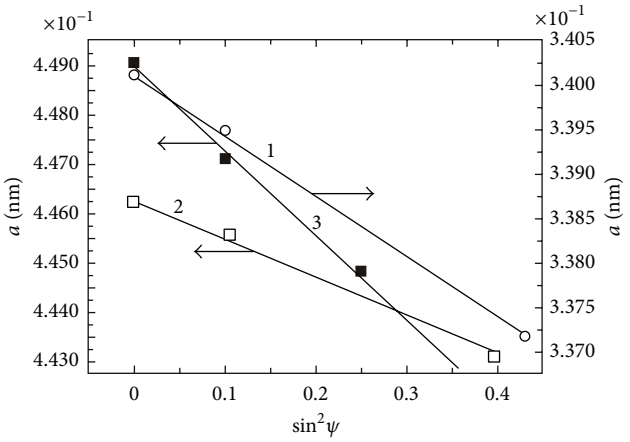

FIGURE 6: Dependences of α-$\sin^2\psi$ obtained for the texture axis (110) of a highentropy alloy Ti-V-Zr-Nb-Hf deposited in a nitrogen-free atmosphere (1), for the texture axis (111) (a straight line 2) and (110) (a straight line 3), which was the coating of the highest hardness (58–60) GPa deposited in the nitrogen atmosphere at $P_N = 0.27$ Pa and $U_b = -200$ V, using a method of crystalline groups.

the FCC sublattice shifted by 1/2 space diagonal forming the so-called NaCl structural lattice type. The appearance of reflections at small angles was also observed, corresponding to the formation of oxides of TiO_2 (JCPDS 01-0562) and oxide-type $MeTiO_4$, where Me corresponds to the content of Zr and Hf. The structural type of this oxide is similar to an oxide of an isostructural (allomeric) $ZrTiO_4$ (JCPDS 07-0290) and $HfTiO_4$ (JCPDS 14-0103). Upon annealing of the sample, the strain state of compression decreased from –1.9% (before annealing) to –0.7% (after annealing).

A characteristic form of α-$\sin^2\psi$ plots for highentropy metallic coating with a bcc lattice and a nitride one with an FCC metallic lattice of NaCl type is demonstrated in Figure 6. We can see that a compressing deformation exceeding 2% was developing in the CAVD coatings. Inclination angles of the plots are different for all investigated nitride coatings and crystalline groups of definite textures in this work (Figure 6, plots 2 and 3). According to Roy's model of stress uniformity [25, 33], such difference indicates an essential contribution of oriented microstresses of the deformation mode, surveyed by the α-$\sin^2\psi$ method. In this case, if a region of the uniform microdeformation is comparable to the crystallite size, the latter demonstrates anisotropy of an elastic modulus. In the case of complexes of textured crystallites, such deformation can be considered as a factor of nonuniformity of stresses and deformations due to intercrystalline interactions [31, 34]. Measurements of the material elastic characteristics, which were performed using the macro- and microbeams and calculated according to the Vergard's rule, along with the element analysis indicated that a period of crystalline lattice was about 0.3371 nm for the highentropy coating $Ti_{0.23}$-$V_{0.05}$-$Zr_{0.07}$-$Hf_{0.078}$-$N_{0.49}$. This value corresponds to that of the stress-free cross-section $2\nu/(1+\nu) = 0.45$ in terms of the plotted for this coating α-$\sin^2\psi$ (plot 1, Figure 6), where ν is the Poisson coefficient. From here $\nu = 0.29$, and the elastic strain of compression developing in such coating has the value 2.2 GPa. The previously mentioned approach can be applied for calculations of stresses in the nitride single-axis oriented coatings. In the case of double-axis-orientation (plots 2 and 3, Figure 6), application of averaged meaning allows us only to perform a correct evaluation of the deformed state of the crystal lattice.

The results of RBS (Figures 2(a) and 2(b)) and EDX analyses for the samples 510 (for which the value of the

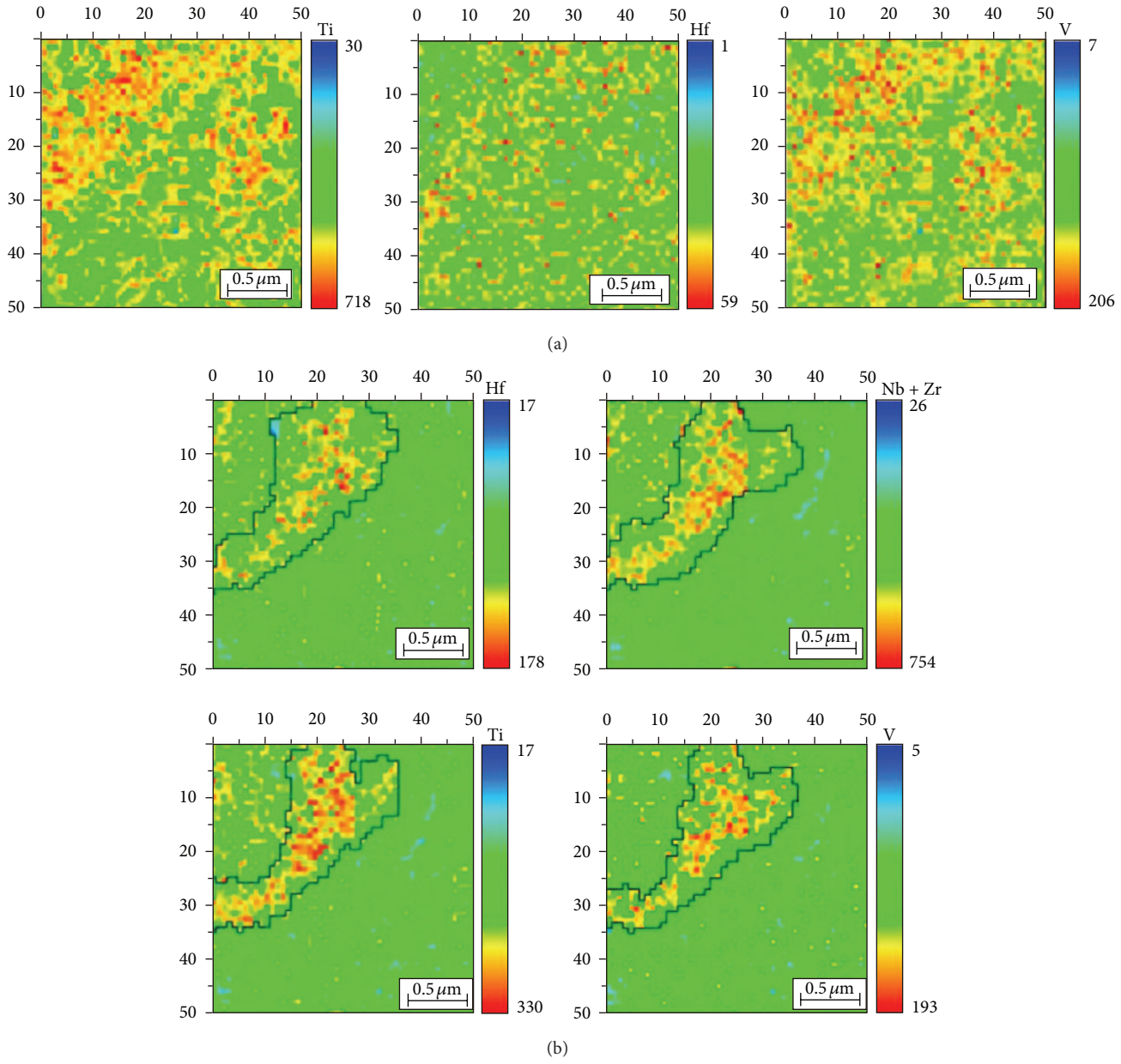

FIGURE 7: Maps of the element distribution in the area of 2.5 × 2.5 μm (the raster of 50 × 50, the step size of 0.5 μm) for the sample 512 before (a) and after (b) annealing.

elastic stress in the initial state is much lower than for sample 512) indicated that two peaks are formed on the curve of S-parameter when the energy of the positron beam is (3 ÷ 5) keV and (14 ÷ 17) keV. This can be explained by the increased diffusion process of both nitrogen and oxygen atoms near the surfaces of the samples 510. This indicates the appearance of new channels for the annihilation of positrons, which are more efficiently attracted by defects, which appeared at the interface as a result of annealing and formed the new quasi-amorphous and nanostructured phases of nitrides. This conclusion is supported by the results of PIXE-μ analysis, which indicated that an oxide film was formed on the surface, and therefore the value of S-parameter increased. In the coating depth, the elements are redistributed, which confirmed the assumption about the end of the process of spinodal segregation and the formation of new phases along nanograin interfaces [30–34]. It must be noted that the grain growth during annealing is the most obvious mechanism of structural relaxation. The segregation of nitrogen at the grain interfaces hampers the growth of nanocrystals.

Evaluation of the nanograins size by XRD, according to the Debye-Scherrer, gave the nanograins size of 55–58 nm for samples 512, which did not change after thermal annealing. Evaluation of the diffusion length of positrons was L + ≈ 100 nm, which was essentially longer than the size of

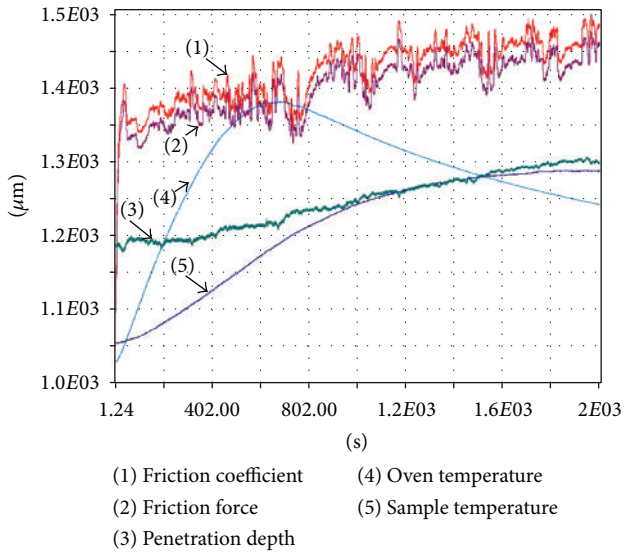

Figure 8: Results of tribological tests of steel substrate (steel 45).

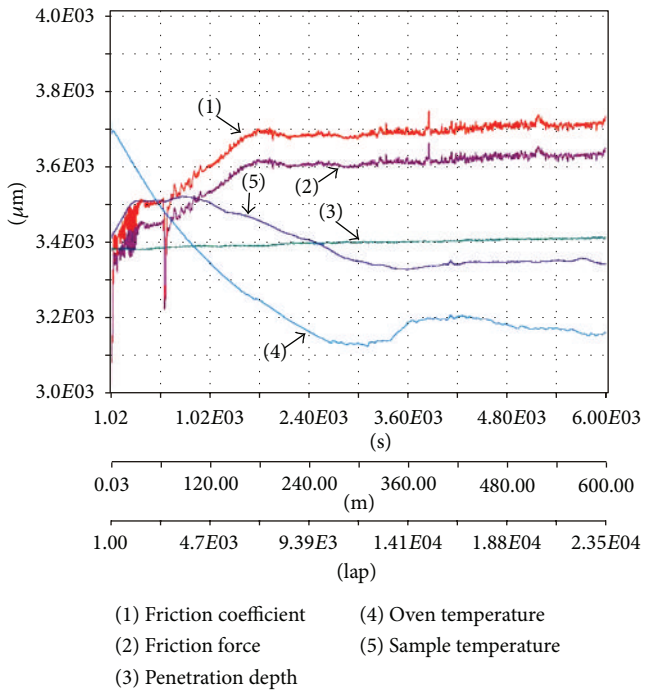

Figure 9: The results of tribological tests of the "steel 45 + coating (Ti-HF-Nb-Zr-V)N-Al_2O_3 counterface."

nanograins. According to the conventional interpretation, the nanopores are primarily placed at the lines of intersection of three or more interfaces. Thus, the ratio of intensities of the positron lifetime components should decrease with the increase of crystallite size. It was confirmed by the theoretical and experimental studies [27–29, 33]. Therefore, reduction of the *S*-parameter (sample 512) may be connected to the annealing of interface vacancies, resulting in a decrease of the *S*-parameter intensity [38–40].

Moreover, additional nanopores may appear due to the vacancy agglomeration taking place in the process of crystallite growing, even if the latter is not very significant. This may result in the increase of the *S*-parameter. This was reported in the work of [32], where the intensity of the second component of positron lifetime increased.

As it follows from the RBS (Figures 2(a) and 2(b)) and EDX analyses, the strongly structured coatings number 512 with a high level of compressive strain in the as-deposited states (−2.76%) demonstrate the high oxidation resistance after annealing. This occurred due to low oxygen diffusion to the coating depth and a high degree of filling of the octahedral interstitials by nitrogen atoms during the deposition of coating under conditions of high nitrogen pressure in the chamber. Thus, this system does not form a nitride interlayer between nanograins, due to the low diffusion resulting from high compressive stresses. It seems that the annealing temperature is insufficient or the energy of atoms is too low to form the interlayer. Therefore, the main channel allowing the nitrogen atoms to sink for the formation of the nitride interlayer is the interphase "coating substrate" boundary (see the *S*-parameter curve of the maximum value 0.53 at energy of analyzing positron beam of 13-14 keV).

Figure 7(a) shows the 3D map of the element distribution in the area of 2.5 × 2.5 μm for the sample 512, with scanning step 0.5 μm. As we can see in this figure, the elements are distributed almost evenly over the surface and in the bulk. At the same time, thermal annealing up to 873 K (for 30 min, at pressure in chamber 100 Pa) leads to the segregation of impurities at the grain interfaces, and the maps of these distributions clearly indicate these regions, see Figure 7(b). We pay attention to the fact that almost all the elements forming the coating are arranged, and since the method PIXE is insensitive to nitrogen, the spectrum does not indicate it. The width of these interfaces is about 0.12 ± 0.25 μm, and the size of large grains reaches up to 0.3–0.8 μm. Thus, considering the results of XRD analysis and μ-PIXE with *S*-parameter before and after annealing, we can say that in the structure of (Ti-Zr-Hf-V-Nb)N the grains of 0.3–0.8 μm with nanograins of 45–60 nm fragmented into them are formed. Dimensions of these nanograins were determined by XRD. After annealing, the impurities are segregated at the interfaces of large grains due to thermostimulated diffusion, and an interphase interlayer is formed at small grains as an agglutinating phase.

The results of research obtained by electron diffraction microscope (TEM) demonstrated that the structural-phase state of coatings with different contents of alloying elements (Si, B, Al) in the system TiN even at high diffusion mobility of atoms (i.e., at deposition temperature 673–773 K) formed the two-phase textured grain structures. The grains of a submicron size 0.2–0.6 μm in such systems were fragmented by the low-angle interfaces with the disorientation angles of 5° and by nanograins of 20–30 nm [13].

According to [12, 13, 17], increasing of content of low-soluble alloying elements, upon reaching their critical concentration and/or diffusion mobility, leads to enrichment of interfaces of growing crystals with these elements (taking into account the values of mixing entropy of separate nitrides,

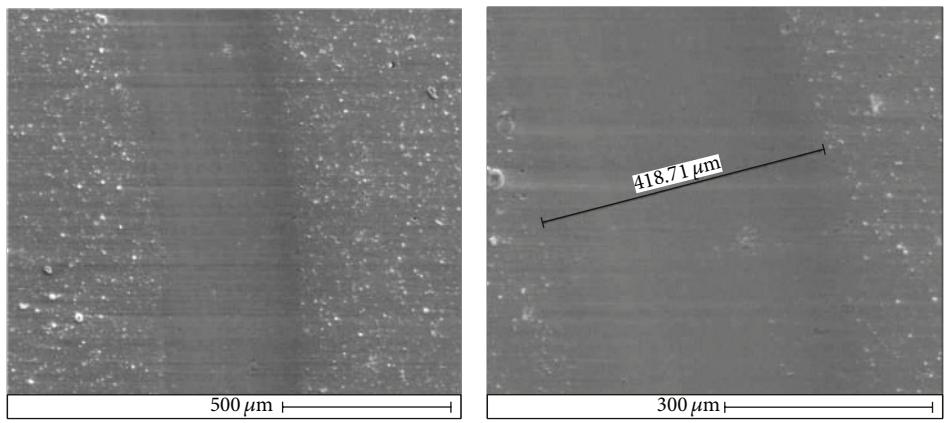

Figure 10: Photographs of the surface morphology of friction: (a) general view and (b) friction track.

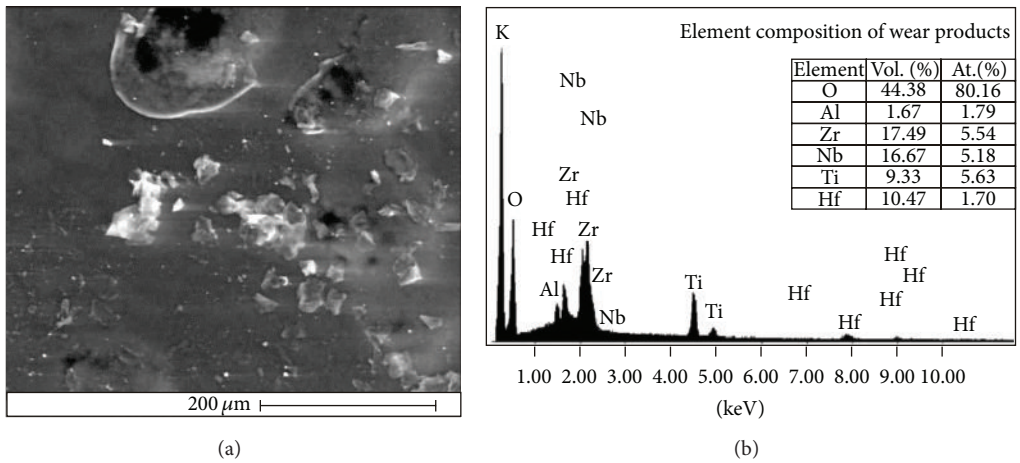

Figure 11: Micrograph of wear products (a) and and its energy spectrum (b).

Table 2: The enthalpies of formation (ΔH) of the five binary nitrides.

	TiN	VN	ZrN	HfN	NbN
ΔH, KJ/mole	−337.7	−217.2	365.3	−373	−234.7

presented in Table 2, and also the total entropy of all metals and nitrides on its basis included to the coatings), and to corresponding decrease of the grain size [41]. This effect, along with the nonequilibrium deposition conditions, promoted the formation of randomly oriented nanocrystallites. It should be noted that the maximum nanohardness of H = 58 GPa was obtained also for the samples 512. Elastic modulus for these samples reached the value of E = 618 GPa. For samples 509 and 510, hardness values were of little lower rates −52 GPa and 46 GPa, respectively.

Analysis of the wear byproducts, wear track structure (on the sample), and wear spots (on counterface ball) was provided along with microscopic study of the wear tracks structure on the coating surface and the change of wear spots on the ball. Measurement of the vertical section of wear tracks was performed by profilometer in four diametrically and orthogonally opposite fields and determined the average cross-sectional area and wear tracks. Figure 8 presents the results of tribological wear test of the steel substrate. The vacuum-arc coatings of Ti-Zr-Hf-Nb-V (4.0 mm thick) were deposited in the nitrogen reaction gas environment on the polished steel disc. The results of the friction tests showed the increase of the surface roughness due to the drop component of the plasma flow (see Figure 9 and Table 3).

Deposition of coatings on the substrate of steel 45 provides an increased durability, thus reducing the wear of steel. The study of friction tracks is of great interest, which can give the information about the mechanism of wear. Figure 10 shows photographs of friction tracks in vacuum-arc coating (Ti-HF-Nb-Zr-V)N. Results of the study of wear products in the friction process for the coating (Ti-HF-Nb-Zr-V)N-Al_2O_3 counterface are shown in Figure 11.

Table 3: Tribological characteristics of the different systems based on Ti, Zr, Hf, Nb, V, N.

Sample	Friction coefficient, μ		Wear factor $mm^3 \times H^{-1} \times mm^{-1}$	
	Initial	During experiment	Of counterface ($\times 10^{-5}$)	Of sample ($\times 10^{-5}$)
Coatings Ti-Hf-Nb-Zr-V-N	0.221	1.030	1.12	0.027
Steel 45	0.204	0.674	0.269	35.36

4. Conclusion

Present work reports original results revealing the mechanisms of formation of interfaces in multicomponent coatings and formation of the stress states of nanocrystals, as well as their effect on thermal diffusion of nitrogen and oxygen atoms. We found that by changing the deposition conditions, it is possible to influence on thermal stability and hardness of multicomponent nanostructured coatings.

We also considered an effect of defect migration, which occurs in the process of annealing, on hampering the nanocrystal growing, when the annealing temperature increased. It turned out that the highentropy nitride alloys and nanostructured coatings on their base contained only the single-phase solid solutions. Its structure was composed of the submicron grains of 0.3–0.8 μm, at the interfaces of which the interlayers of impurity atoms were formed. At the same time, the fragmented nanograin structures of 40–60 nm size with subgrains of the nitride phases were formed in the submicron grains. The sluggish diffusion originating from the higher packing density because of the packing of atoms with different sizes made the effective diffusion distances very short, which led to the enhanced difficulty of grain growth. Regarding the lattice decline, the following three possible factors must be considered: composition variation, phase separation, and residual stress.

Acknowledgments

This work was supported by the Ministry of Education and Science, Youth and Sports of Ukraine in the framework of the state program (order no. 411) and in collaboration with the National Institute of Material Science, Tsukuba, and Japan, Martin-Luther Universitat Halle-Wittenberg, and Ion Beam Center FWIZ, Dresden, and partially by the Project FRSF-041/20, Ukraine. The author is grateful to V. F. Gorban, S. A. Firstova, and A. A. Andreev, for the help in preparation of coatings, to S. S. Mel'nik, for the help in providing of experiments on proton microbeam, and to Professor R. Krause-Rehberg, M. Jungman, M. Muchow, and J. Haeberle and Martin-Luther-Universitat Halle-Wittenberg, Halle, Germany, and M. Kaverin for the help in research using slow positron beam, to Professor Sobol O. V., for the help in providing of XRD analysis and "α-$\sin^2\psi$" analysis, to Professor Beresnev V. M., for the help in interpretation of nanoscratch tests, to Dr. Kolesnikov D. A. Belgorod State University, Nano-Center, Russia, and to Professor Y. Takeda from NIMS, Tsukuba, Japan, for the help in providing of SIMS with EDX measurements.

References

[1] A. D. Pogrebnjak, A. P. Shpak, N. A. Azarenkov, and V. M. Beresnev, "Structures and properties of hard and superhard nanocomposite coatings," *Physics-Uspekhi*, vol. 52, no. 1, pp. 29–54, 2009.

[2] A. D. Pogrebnjak, A. G. Ponomarev, A. P. Shpak, and Y. A. Kunitskii, "Application of micro- and nanoprobes to the analysis of small-sized 3D materials, nanosystems, and nanoobjects," *Physics-Uspekhi*, vol. 55, no. 3, pp. 270–300, 2012.

[3] A. D. Pogrebnjak, V. M. Beresnev, A. A. Demianenko et al., "Adhesive strength, superhardness, and the phase and elemental compositions of nanostructured coatings based on Ti-Hf-Si-N," *Physics of the Solid State*, vol. 54, no. 9, pp. 1882–1890, 2012.

[4] A. D. Pogrebnjak, O. V. Sobol', V. M. Beresnev et al., "Features of the structural state and mechanical properties of ZrN and Zr(Ti)-Si-N coatings obtained by ion-plasma deposition technique," *Technical Physics Letters*, vol. 35, no. 10, pp. 925–928, 2009.

[5] V. Dolique, A.-L. Thomann, P. Brault, Y. Tessier, and P. Gillon, "Complex structure/composition relationship in thin films of AlCoCrCuFeNi high entropy alloy," *Materials Chemistry and Physics*, vol. 117, no. 1, pp. 142–147, 2009.

[6] M.-H. Tsai, C.-W. Wang, C.-W. Tsai et al., "Thermal stability and performance of NbSiTaTiZr high-entropy alloy barrier for copper metallization," *Journal of the Electrochemical Society*, vol. 158, no. 11, pp. H1161–H1165, 2011.

[7] A. Li and X. Zhang, "Thermodynamic analysis of the simple microstructure of AlCrFeNiCu high-entropy alloy with multi-principal elements," *Acta Metallurgica Sinica*, vol. 22, no. 3, pp. 219–224, 2009.

[8] S. A. Firstov, V. F. Gorban, N. A. Krapivka, and E. P. Pechkovsky, "Hardening and mechanical properties of as-cast high-entropy alloys," *Composites and Nanostures*, vol. 2, pp. 5–20, 2011.

[9] A. D. Pogrebnjak, V. V. Uglov, M. V. Il'yashenko et al., "Nano-microcomposite and combined coatings on Ti-Si-N/WC-Co-Cr/steel and Ti-Si-N/$(Cr_3C_2)_{75}$-$(NiCr)_{25}$ base: their structure and properties," in *Nanostructured Materials and Nanotechnology IV: Ceramic Engineering and Science Proceedings*, vol. 31, pp. 115–126, John Wiley & Sons, Hoboken, NJ, USA, 2010.

[10] O. V. Sobol', A. D. Pogrebnjak, and V. M. Beresnev, "Effect of the preparation conditions on the phase composition, structure, and mechanical characteristics of vacuum-Arc Zr-Ti-Si-N coatings," *The Physics of Metals and Metallography*, vol. 112, no. 2, pp. 188–195, 2011.

[11] J. Musil, J. Vlček, and P. Zeman, "Hard amorphous nanocomposite coatings with oxidation resistance above 1000°C," *Advances in Applied Ceramics*, vol. 107, no. 3, pp. 148–154, 2008.

[12] A. D. Korotaev, D. P. Borisov, V. Y. Moshkov, S. V. Ovchinnikov, Y. P. Pinzhin, and A. N. Tyumentsev, "Elastic stress state in superhard multielement coatings," *Physical Mesomechanics*, vol. 12, no. 5-6, pp. 269–279, 2009.

[13] A. D. Pogrebnjak, V. M. Beresnev, D. A. Kolesnikov et al., "The effect of segregation and thermodiffusion on the formation of interfaces in nanostructured (Ti-Hf-Zr-V-Nb)N multielement coatings," *Technical Physics Letters*, vol. 39, no. 3, pp. 280–283, 2013.

[14] O. V. Sobol', A. A. Andreev, V. F. Gorban et al., "Reproducibility of the single-phase structural state of the multielement high-entropy Ti-V-Zr-Nb-Hf system and related superhard nitrides formed by the vacuum-arc method," *Technical Physics Letters*, vol. 38, no. 7, pp. 616–619, 2012.

[15] I. V. Blinkov, A. O. Volkhonsky, V. N. Anikin, M. I. Petrzhik, and D. E. Derevtsova, "Phase composition and properties of wear-resistant Ti-Al-Cr-Zr-Nb-N PVD coatings," *Physics and Chemistry of Materials Processing*, vol. 4, pp. 37–43, 2010 (Russian).

[16] S.-Y. Lin, S.-Y. Chang, Y.-C. Huang, F.-S. Shieu, and J.-W. Yeh, "Mechanical performance and nanoindenting deformation of (AlCrTaTiZr)NCy multi-component coatings co-sputtered with bias," *Surface and Coatings Technology*, vol. 206, no. 24, pp. 5096–5102, 2012.

[17] J. Musil, "Hard nanocomposite coatings: thermal stability, oxidation resistance and toughness," *Surface and Coatings Technology*, vol. 207, pp. 50–65, 2012.

[18] A. D. Pogrebnjak and V. M. Beresnev, *Nanocoatings Nanosystems Nanotechnologies*, Bentham Science, 2012.

[19] A. D. Pogrebnjak, A. P. Shpak, V. M. Beresnev et al., "Effect of thermal annealing in vacuum and in air on nanograin sizes in hard and superhard coatings Zr-Ti-Si-N," *Journal of Nanoscience and Nanotechnology*, vol. 12, pp. 9213–9219, 2012.

[20] H.-W. Chang, P.-K. Huang, J.-W. Yeh, A. Davison, C.-H. Tsau, and C.-C. Yang, "Influence of substrate bias, deposition temperature and post-deposition annealing on the structure and properties of multi-principal-component (AlCrMoSiTi)N coatings," *Surface and Coatings Technology*, vol. 202, no. 14, pp. 3360–3366, 2008.

[21] C.-H. Lai, K.-H. Cheng, S.-J. Lin, and J.-W. Yeh, "Mechanical and tribological properties of multi-element (AlCrTaTiZr)N coatings," *Surface and Coatings Technology*, vol. 202, no. 15, pp. 3732–3738, 2008.

[22] C.-H. Lai, M.-H. Tsai, S.-J. Lin, and J.-W. Yeh, "Influence of substrate temperature on structure and mechanical, properties of multi-element (AlCrTaTiZr)N coatings," *Surface and Coatings Technology*, vol. 201, no. 16-17, pp. 6993–6998, 2007.

[23] J.-W. Yeh, Y.-L. Chen, S.-J. Lin, and S.-K. Chen, "High-entropy alloys—a new era of exploitation," *Materials Science Forum*, vol. 560, pp. 1–9, 2007.

[24] http://www.simnra.com.

[25] N. A. Azarenkov, O. V. Sobol', A. D. Pogrebnjak, and V. M. Beresnev, *Engineering Vacuum-Plasma Coatings*, Academy of Kyungpook National University, Kharkov, Ukraine, 2011.

[26] H. E. Shaefer, "Investigation of thermal equilibrium vacancies in metals by positron annihilation," *Physica Status Solidi*, vol. 102, no. 1, pp. 47–65, 1987.

[27] S. V. Rempel' and A. I. Gusev, "Surface segregation in decomposing carbide solid solutions," *JETP Letters*, vol. 88, no. 7, pp. 435–440, 2008.

[28] R. Würschum, P. Farber, R. Dittmar, P. Scharwaechter, W. Frank, and H.-E. Schaefer, "Thermal vacancy formation and self-diffusion in intermetallic Fe_3Si nanocrystallites of nanocomposite alloys," *Physical Review Letters*, vol. 79, no. 24, pp. 4918–4921, 1997.

[29] V. I. Lavrent'yev, A. D. Pogrebnjak, and R. Sandrik, "Evolution of vacancy defects in the surface layers of a metal irradiated with a pulsed electron beam," *JETP Letters*, vol. 65, no. 8, pp. 651–655, 1997.

[30] S. Vepřek, "The search for novel, superhard materials," *Journal of Vacuum Science & Technology A*, vol. 17, no. 5, pp. 2401–2421, 1999.

[31] J. Musil, "Hard and superhard nanocomposite coatings," *Surface and Coatings Technology*, vol. 125, no. 1–3, pp. 322–330, 2000.

[32] A. I. Gusev, *Nanomaterials, Nanostructures and Nanotechnology*, Fizmatlit, Moscow, Russia, 2005.

[33] R. Krause-Rehberg and H. S. Leipner, *Positron Annihilation in Semiconductors*, vol. 127 of *Solid-State Sciences*, Springer, Berlin, Germany, 1999.

[34] A. D. Pogrebnjak, A. G. Ponomarev, D. A. Kolesnikov et al., "Effect of mass transfer and segregation on the formation of superhard nanostructured Ti-Hf-N(Fe) catings," *Technical Physics Letters*, vol. 38, no. 7, pp. 623–626, 2012.

[35] S.-Y. Chang, S.-Y. Lin, Y.-C. Huang, and C.-L. Wu, "Mechanical properties, deformation behaviors and interface adhesion of (AlCrTaTiZr)Nx multi-component coatings," *Surface and Coatings Technology*, vol. 204, no. 20, pp. 3307–3314, 2010.

[36] P.-K. Huang and J.-W. Yeh, "Effects of nitrogen content on structure and mechanical properties of multi-element (AlCrNbSiTiV)N coating," *Surface and Coatings Technology*, vol. 203, no. 13, pp. 1891–1896, 2009.

[37] D.-C. Tsai, Y.-L. Huang, S.-R. Lin, S.-C. Liang, and F.-S. Shieu, "Effect of nitrogen flow ratios on the structure and mechanical properties of (TiVCrZrY)N coatings prepared by reactive magnetron sputtering," *Applied Surface Science*, vol. 257, no. 4, pp. 1361–1367, 2010.

[38] A. D. Pogrebnjak, O. V. Sobol', V. M. Beresnev et al., "Phase composition, thermal stability, physical and mechanical properties of superhard on base Zr-Ti-Si-N nanocomposite coatings," *Ceramic Engineering and Science Proceedings*, vol. 31, no. 7, pp. 127–138, 2010.

[39] A. D. Pogrebnjak, S. M. Ruzimov, D. L. Alontseva et al., "Structure and properties of coatings on Ni base deposited using a plasma jet before and after electron a beam irradiation," *Vacuum*, vol. 81, no. 10, pp. 1243–1251, 2007.

[40] A. D. Pogrebnjak, O. G. Bakharev, N. A. Pogrebnjak Jr. et al., "Certain features of high-dose and intensive implantation of Al ions in iron," *Physics Letters A*, vol. 265, no. 3, pp. 225–232, 2000.

[41] P. Misaelides, A. Hatzidimitriou, F. Noli, E. Pavlidou, and A. D. Pogrebnjak, "Investigation of the characteristics and corrosion resistance of Al_2O_3/TiN coatings," *Applied Surface Science*, vol. 252, no. 23, pp. 8043–8049, 2006.